The new oxide paradigm for solid state ultraviolet photodetectors

D. J. Rogers, P. Bove, X. Arrateig, V. E. Sandana, F. H. Teherani, et al.

D. J. Rogers, P. Bove, X. Arrateig, V. E. Sandana, F. H. Teherani, M. Razeghi, R. McClintock, E. Frisch, S. Harel, "The new oxide paradigm for solid state ultraviolet photodetectors," Proc. SPIE 10533, Oxide-based Materials and Devices IX, 105331P (22 March 2018); doi: 10.1117/12.2319505

SPIE.

Event: SPIE OPTO, 2018, San Francisco, California, United States

The New Oxide Paradigm for Solid State Ultraviolet Photodetectors

D. J. Rogers[1*], P. Bove[1], X. Arrateig[1], V. E. Sandana[1], F. H. Teherani[1]
M. Razeghi[2], R. McClintock[2], E. Frisch[3] & S. Harel[3]

[1] Nanovation, 8 route de Chevreuse, 78117 Châteaufort, France
[2] Center for Quantum Devices, ECE Department, Northwestern University, Evanston, USA
[3]Ofil Systems, Einstein St., Weizmann Science Park, Ness Ziona 74140, Israel
*E-mail: rogers@nanovation.com

ABSTRACT

The bandgap of wurzite ZnO layers grown on 2 inch diameter c-Al_2O_3 substrates by pulsed laser deposition was engineered from 3.7 to 4.8 eV by alloying with Mg. Above this Mg content the layers transformed from single phase hcp to mixed hcp/fcc phase before becoming single phase fcc above a bandgap of about 5.5 eV. Metal-Semiconductor-Metal (MSM) photodetectors based on gold Inter-Digitated-Transducer structures were fabricated from the single phase hcp layers by single step negative photolithography and then packaged in TO5 cans. The devices gave over 6 orders of magnitude of separation between dark and light signal with solar rejection ratios (I_{270} : I_{350}) of over 3 x 10^5 and dark signals of 300 pA (at a bias of -5V). Spectral responsivities were engineered to fit the "Deutscher Verein des Gas- und Wasserfaches" industry standard form and gave over two decade higher responsivities (14 A/W, peaked at 270 nm) than commercial SiC based devices. Homogeneous Ga_2O_3 layers were also grown on 2 inch diameter c-Al_2O_3 substrates by PLD. Optical transmission spectra were coherent with a bandgap that increased from 4.9 to 5.4 eV when film thickness was decreased from 825 to 145 nm. X-ray diffraction revealed that the films were of the β-Ga_2O_3 (monoclinic) polytype with strong (-201) orientation. β-Ga_2O_3 MSM photodetectors gave over 4 orders of magnitude of separation between dark and light signal (at -5V bias) with dark currents of 250 pA and spectral responsivities of up to 40 A/W (at -0.75V bias). It was found that the spectral responsivity peak position could be decreased from 250 to 230 nm by reducing film thickness from 825 to 145 nm. This shift in peak responsivity wavelength with film thickness (a) was coherent with the apparent bandgap shift that was observed in transmission spectroscopy for the same layers and (b) conveniently provides a coverage of the spectral region in which MgZnO layers show fcc/hcp phase mixing.

1. INTRODUCTION

Solid state ultraviolet (UV) photodetectors (PD) are projected for detection of weak UV signals in applications such as chemical threat detection, next-generation missile warning systems, hostile fire identification, missile guidance, flame/chemical/biological-agent detection, environmental monitoring and non-line-of-sight communications. To minimize false alarms and background clutter many of these systems operate in the solar-blind (SB) portion of the UV spectrum (<290 nm) [1]. Most current SB systems are usually based on photomultiplier tubes (PMTs) with Cs_2Te photocathodes. These have a detection tail out to 325 nm, however, which overlaps with the solar

Oxide-based Materials and Devices IX, edited by David J. Rogers, David C. Look,
Ferechteh H. Teherani, Proc. of SPIE Vol. 10533, 105331P · © 2018 SPIE
CCC code: 0277-786X/18/$18 · doi: 10.1117/12.2319505

UV spectrum making these sensors not truly blind to solar background radiation. Thus filters and complex optics are usually required to achieve true solar-blindness. The existing detectors have a peak detective quantum efficiency of 15% at best. In addition, the high voltage vacuum tubes are bulky, fragile (mechanically and electrically – high flux can physically damage the internal electron multiplication grids) expensive and require high operating voltages. Solid-state SBPDs promise performance, size and cost advantages compared to PMTs. Such arrays have no moving parts, are intrinsically radiation hard and potentially offer higher quantum efficiency, higher selective sensitivity, extended lifetimes, lower noise and lower power requirements. Silicon carbide (SiC), with a room-temperature bandgap of 2.4–3.1 eV, is the first wide bandgap semiconductor that has been adopted commercially for use as a basis for deep UV PD and commercial instruments, such as SiC-based flame detectors working in the UVC range, are already available. However, the insertion of optical filters is necessary in such applications in order to tune the photodetecting system to the appropriate spectral range since bandgap engineering through alloying is not possible in SiC. Gallium nitride (GaN), on the other hand, has a bandgap which is tuneable from the near to far UV range through alloying with aluminium and (Al)GaN based devices have been widely explored for detection of UV light in the SB range [2-4]. Being a direct gap semiconductor, the absorption cutoffs for GaN are also very sharp (< 10 nm per decade) compared to existing photocathodes (~25 nm per decade). This allows them to be made significantly more SB while maximizing the capture in the UVC. However, this material system suffers from several key problems: large dislocation densities, low conductivity, and lattice/thermal expansion mismatches (with the dominant sapphire substrate) which lead to cracking, and efficiency fall-off with increasing Al content. The result is that there has been limited success in demonstrating (Al)GaN based SBPDs with low background signals and good quantum efficiencies [5,6]. Hence there is a need for a more suitable system for use in compact solid state detectors in the UVC range and attention has turned to the exploration of oxide based devices. The two main materials systems which have emerged are magnesium doped zinc oxide ((Mg)ZnO) [7,8] and beta gallium oxide (β-Ga_2O_3) [9-12]. (Mg)ZnO is based on wurzite ZnO, which has a direct wide bandgap of ~3.4 eV that can be tuned into the SB range by alloying with MgO (Eg ~7.8eV) [13] as illustrated in Figure 1 [14].

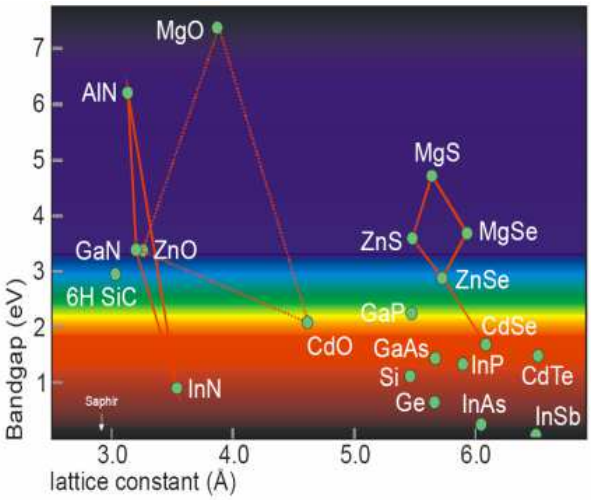

Figure 1. Bandgap engineering possibilities with wide bandgap compound semiconductor materials.

The Mg ion has a similar radius to that of Zn [14], so there are less strain and efficiency drop-off concerns than for AlGaN. As the Mg content increases, however, the hcp ZnO phase transforms into the fcc MgO phase which is much more insulating in nature and less suitable for device applications. Recently there has been a lot of interest in complementing (Mg)ZnO with the even wider bandgap system, β-Ga_2O_3 (Eg ~ 4.9eV). Bandgap engineering further into the UV has also been demonstrated in this material by alloying with Al [15] although no bandgap engineering is necessary in β-Ga_2O_3 in order to obtain basic SB operation. In this talk we explore the performance and the perspectives for Metal-Semiconductor-Metal (MSM) PD based on both (Mg)ZnO and β-Ga_2O_3.

MSM devices were adopted for the study since p-type ZnO and Ga_2O_3 are not available. An MSM-PD is typically made by forming two Schottky contacts in the form of an Inter-Digited-Transducer (IDT) on a lightly doped n-type material, as shown in Figure 2.

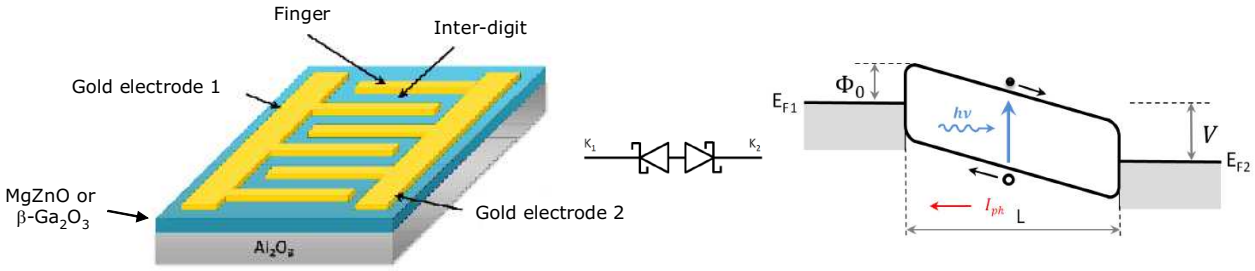

Figure 2 Schematic of the MSM IDT structures adopted in this study along with the corresponding circuit diagram and a band structure representation (adapted from Komla Nomenyo, PhD thesis, "UV Photonics: Top-Down Structuring of ZnO…", 2014).

MSM PDs offer advantages including a single step lithographic fabrication process, relatively low dark currents (due to the rectifying nature of the contacts) the need for only a single homogeneously doped active layer, relatively high speed compared to photoconductor detectors, linearity of photoresponse with optical power, sharp wavelength cut-off, comparatively low parasitic capacitance and low noise. These features make them suitabile for high-bandwidth and monolithic integration without the need for a preamplifier stage. Hence they are attractive for use in aerospace, automotive, military counter measures, petroleum, engine monitoring, flame detection and UVC space astronomy.

2. EXPERIMENT

Figure 3 shows the process flow for the development of a packaged Metal-Semiconductor-Metal (MSM) PD. In figure 3 we can see that there are 5 main steps to achieve a final packaged PD. The first one is the choice of substrate. Sapphire (Al_2O_3) substrates were adopted in this study because the native ZnO and β-Ga_2O_3 substrates are both an order of magnitude more expensive than Al_2O_3 substrates and because they would preclude the study of back illumination operation. (The responsivity of MSM PDs is generally limited by the presence of opaque metal contact electrodes. If the substrate is transparent in the wavelength range of interest, therefore, back illumination can often

provide improved performance through the avoidance of electrode shadowing. This results in lower dark current, more stable contacts and higher quantum efficiency).

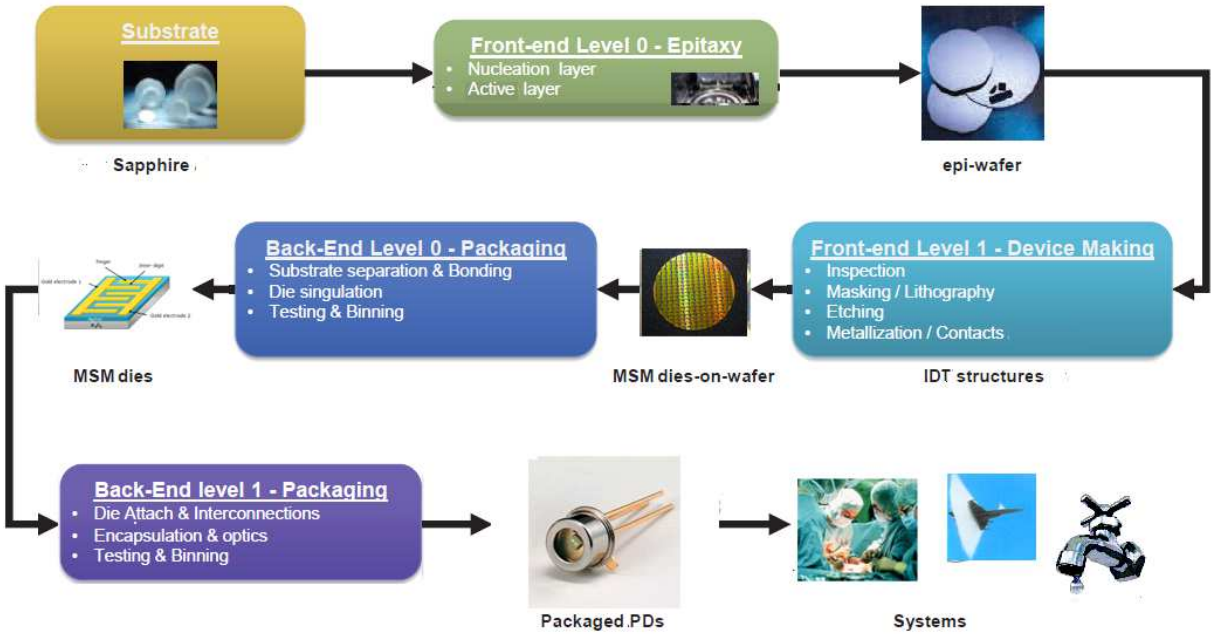

Figure 3: Process flow for the creation of an MSM photodetector (adapted from Yole Developpement).

The second stage of the fabrication is Front End level 0 – Epitaxy. In this study, nominally undoped (Mg)ZnO and β-Ga_2O_3 epilayers were grown by Pulsed Laser Deposition (PLD) from commercial sintered targets using a Coherent LPX KrF (λ = 248nm) laser, as described elsewhere [17,18]. 2 inch diameter wafer coverage was obtained in the PLD growth using optical rastering of the incident laser beam over the target surface.

Optimisation and quality control of the epilayer were done using room temperature (RT) optical transmission studies using an Ocean Optics system comprising a halogen lamp, a deuterium lamp and a Maya optical spectrometer. Film thickness was estimated using optical reflection interferometry with an Ocean Optics Nanocalc system. The crystal structure of the samples was investigated using high resolution X-Ray Diffraction (XRD) performed in a Panalytical MRD Pro system and a Bruker Advance D8 system using Cu $K\alpha_1$ radiation. Electrical resistivity was measured with a Signatone four-collinear-probe system equipped with a Keithley 2400 source-meter. Hall measurements were made at room temperature in Van der Pauw configuration using an Ecopia HMS3000 system with a 1T magnet and indium-soldered Ohmic contacts.

For front-end level 1 MSM PD were fabricated by negative photolithography using Au/Ti IDT with 40 fingers. Finger size was 2 μm x 144 μm and devices with four different finger spacings (2, 4, 6 and 8 μm) were processed and tested.

I/V curves were acquired using a Karl Suss probe station equipped with a Keithley 2400 source meter and an Ocean Optics HPX-2000-HP-DUV 75W Xe fibre optic light source calibrated with an Ophir Nova laser power monitor.

Spectral responsivity spectra were acquired with a Dynasil digital monochromator.

Time response measurements and spectral responsivity were measured with square wave light pulses generated using an optical chopper. A picoscope II digital oscilloscope was used for the measurements.
For back-end level 0, die singulation was achieved by a scribe and dice process using a diamond tip. For back-end level 1, the singulated device die was attached to a TO5 can and wires were bonded to the MSM gold contact pads.

3. RESULTS & DISCUSSION

3.1 MgZnO

3.1.1 MgZnO Front End level 0 – Epitaxy

Figure 4 shows the optical transmission spectra for (Mg)ZnO layers with various Mg contents.

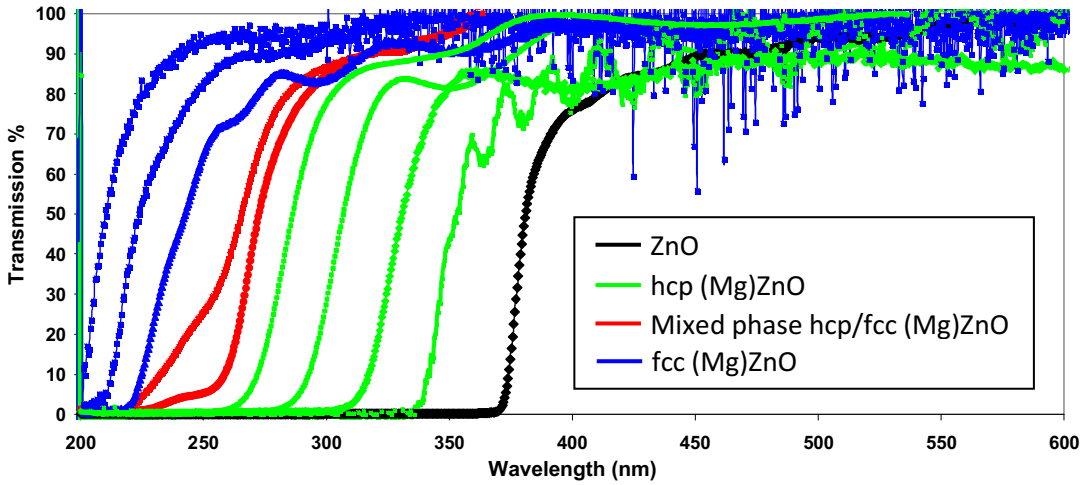

Figure 4 Optical transmission spectra for MgZnO layers with various Mg contents (Mg content increases from right to left).

The figure shows that all layers show good transparency in the visible and a bandgap that increases progressively with increasing Mg content. The layers are single phase hcp from 3.7 to 4.8 eV. Above this Mg content the layers transformed from single phase hcp to mixed hcp/fcc phase before becoming single phase fcc above a bandgap of about 5.5 eV.
Figure 5 summarizes a study into the homogeneity of both the thickness and the optical properties of a typical 2 inch diameter (Mg)ZnO/c-Al_2O_3 wafer showing SB response.

The wafer shows +/- 2% within-wafer variation of the bandgap, +/- 10% within-wafer variation of the film thickness and a good transparency to the visible spectrum.

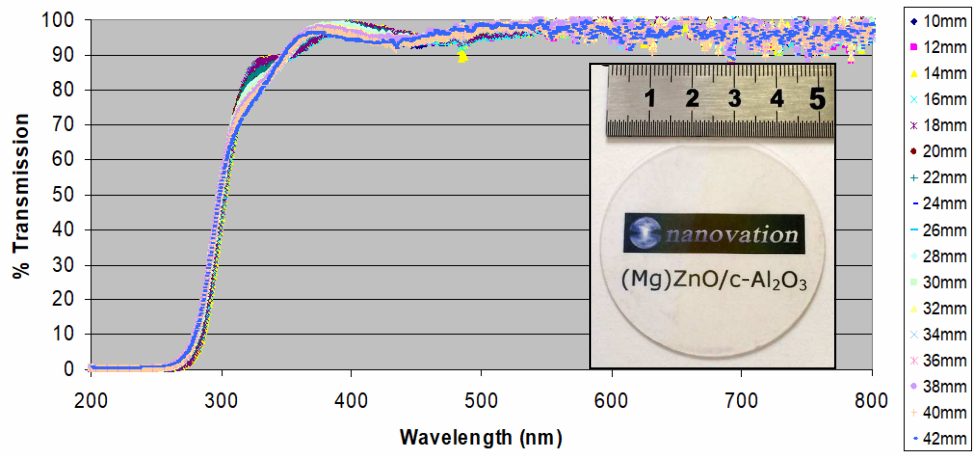

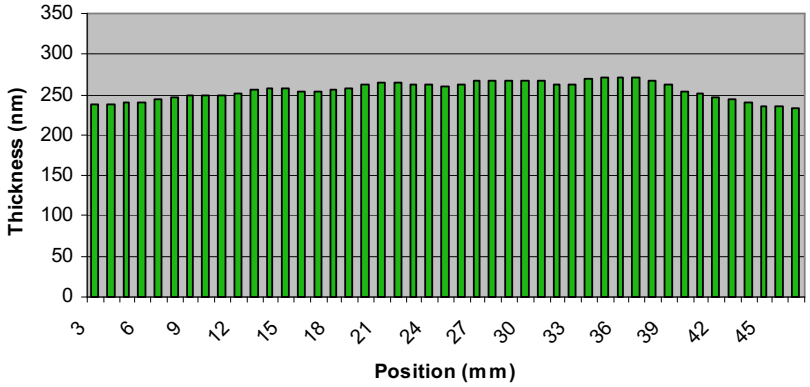

Figure 5 The variation in optical transmission spectra (upper figure) and film thickness (lower figure) across a typical 2 inch diameter hcp MgZnO/c-Al_2O_3 wafer (the inset photograph shows the good transparency to the visible spectrum).

3.1.2 MgZnO Front-end level 1 – Device Processing and Test

Figure 6 shows optical microscope images of typical (Mg)ZnO IDT MSM PD structures.

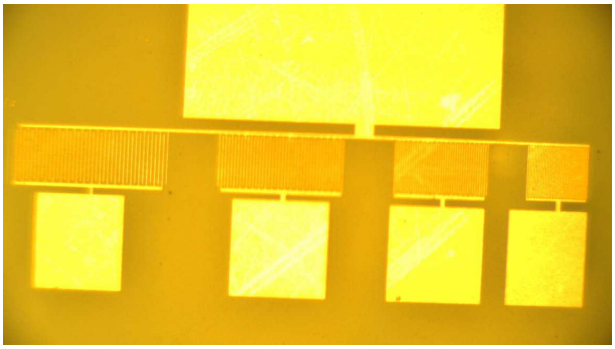

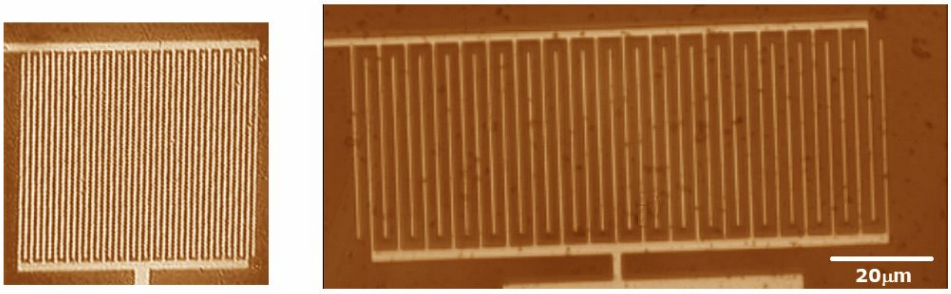

Figure 6 Optical microscope images of (Mg)ZnO IDT MSM PD structures with zooms of patterns having 2 and 8 µm finger spacings, respectively (same scale).

Figure 7 shows typical dependences of the dark and light currents (at -5V bias) on the IDT finger spacing for typical MSM devices based on single phase hcp SB MgZnO/c-Al_2O_3.

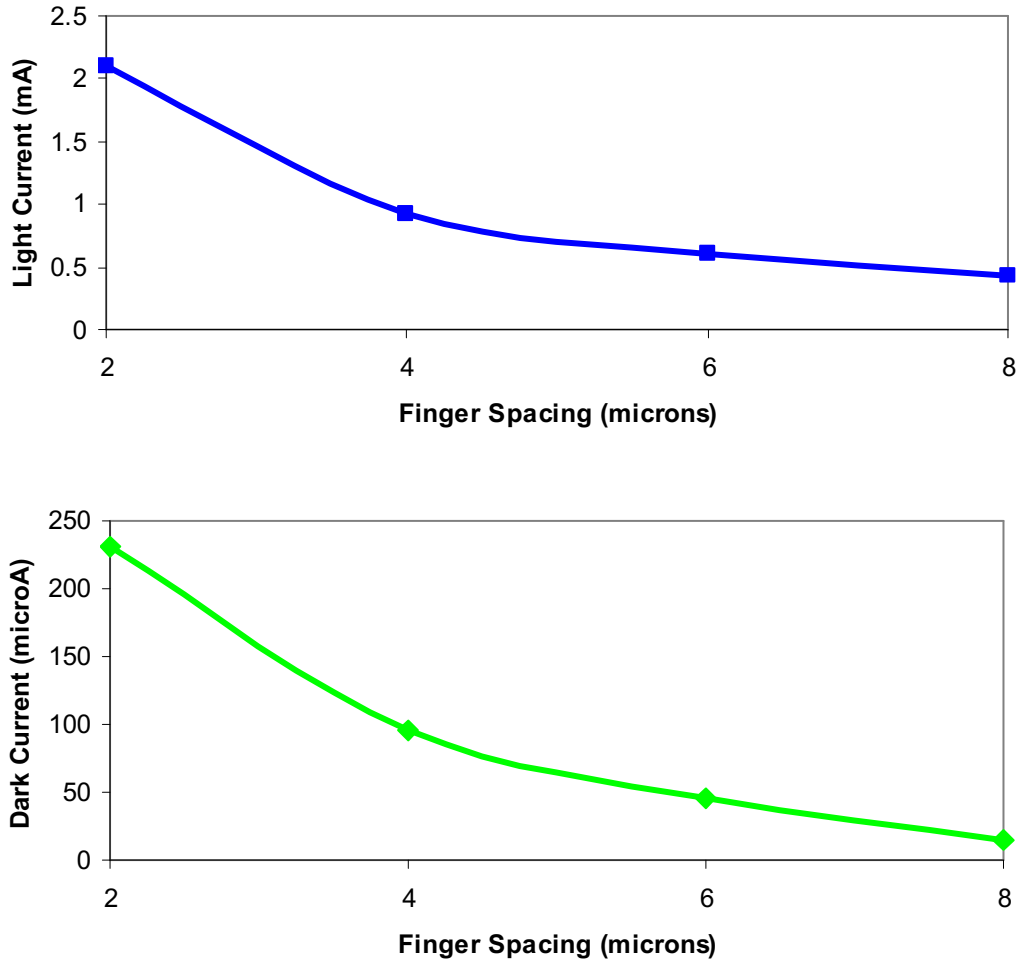

Figure 7 : Evolution of the dark and light current as a function of the IDT finger spacing for MgZnO MSMs with -5V bias (N.B. the two curves are plotted using different scales for current).

Both the dark and light currents decrease with increasing surface area, i.e the interdigit distance. This is coherent with a larger electric field when the voltage bias is fixed but the finger spacing is smaller. Figure 8 shows the evolution of the photocurrent (for the same devices discussed in Figure 7) as a function of IDT finger spacing (for -5V bias).

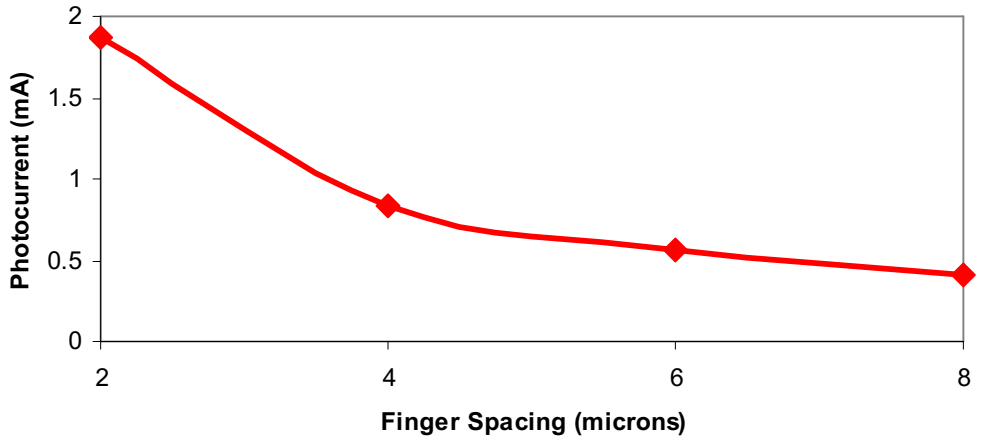

Figure 8 : Evolution of the photocurrent as a function of the finger spacing for SB hcp MgZnO MSMs.

The photocurrent also decreases with increasing surface area. This is as would be expected from Figure 7 since the photocurrent trend is dominated by that of the light current rather than that of the (much smaller) dark current. Figure 9 shows the corresponding dependence of the light/dark ratio on the interdigit distance.

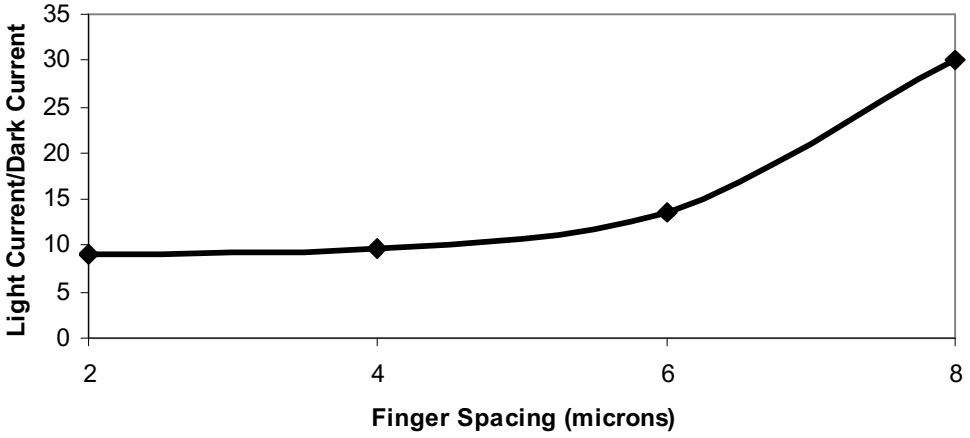

Figure 9: Evolution of the Light/Dark current as a function of the IDT finger spacing for SB hcp MgZnO MSMs.

It can be seen from Figure 9 that the light/dark ratio increases with the interdigit spacing even though the photocurrent is lower. Thus there is a device design trade-off between having higher photocurrent and lower dark signal. Although absolute photocurrent level is also vital, it is important to point out that the achievement of very low dark current (obtained for smaller finger spacings – see Figure 7) is critical to producing UVPDs with a high signal-to-noise ratio (and hence the sensitivity). With regards to the time response of the devices, Figure 10 shows a typical evolution of the 10% / 90% rise/fall time as a function of finger spacing (below saturation frequency).

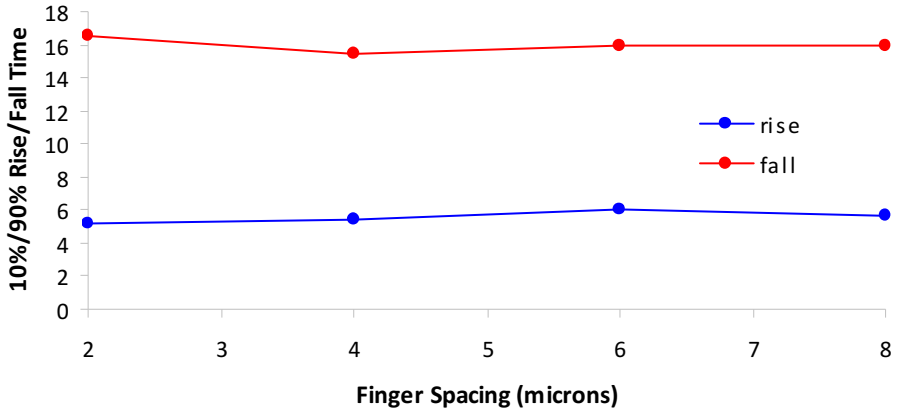

Figure 10 A typical evolution of the 10% / 90% rise/fall time as a function of finger spacing for SB hcp MgZnO based MSMs.

It can be seen that the rise time was generally larger than the fall time and that there was no significant dependence of time response on finger spacing. The rise and fall times were in the few milliseconds range. Figure 11 shows a typical dependence of peak optical responsivity on applied bias voltage for an hcp SB MgZnO based MSM device.

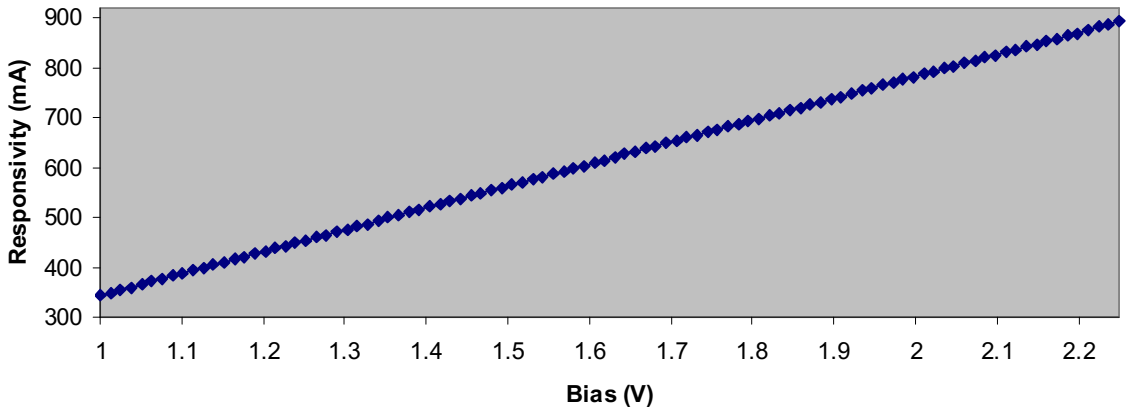

Figure 11 A typical dependence of peak optical responsivity on bias voltage for an (Mg)ZnO based MSM device.

The responsivity is linear with the applied bias, which is as would be expected for an MSM device.

3.1.3 MgZnO Back-end level 1: Device Packaging & Test

$MgZnO/Al_2O_3$ epiwafers were selected for their transmission curves which fitted the "Deutscher Verein des Gas- und Wasserfaches" (DVGW) industry standard spectral response for commercial SiC UVC PDs (see Figures 12 and 13).

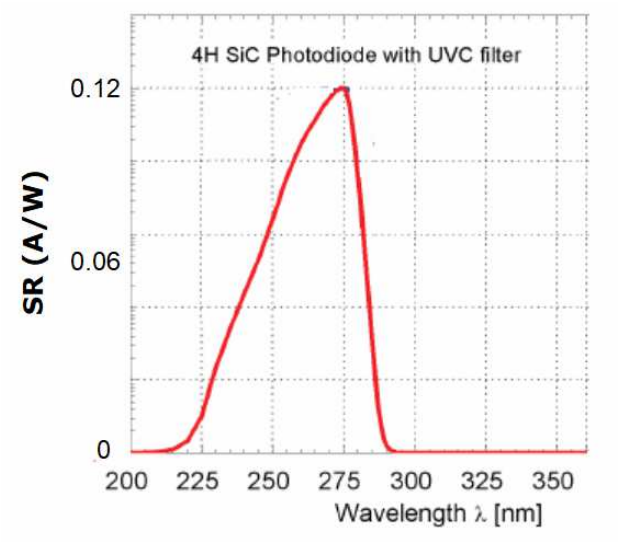

Figure 12 DVGW industry standard spectral response (5V bias) for commercial SiC UVC PDs.

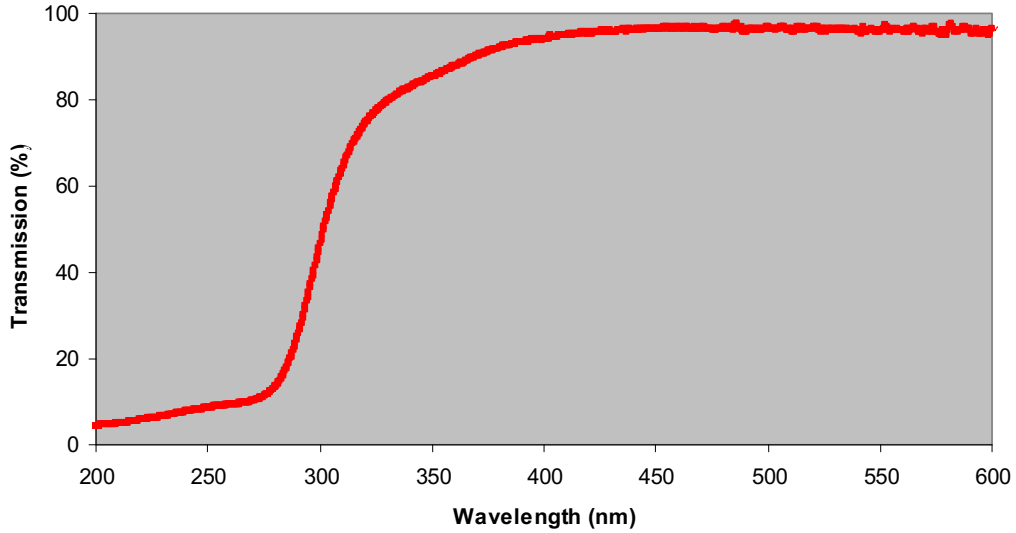

Figure 13 Optical transmission spectrum for an $MgZnO/Al_2O_3$ epiwafer grown by the authors in order to give a match to the spectral response of the DVGW UVC PD standard.

Figure 14 shows I/V curves with/without front illumination for the corresponding (Mg)ZnO MSM device after processing, singulation, wire bonding and mounting in a T05 can.

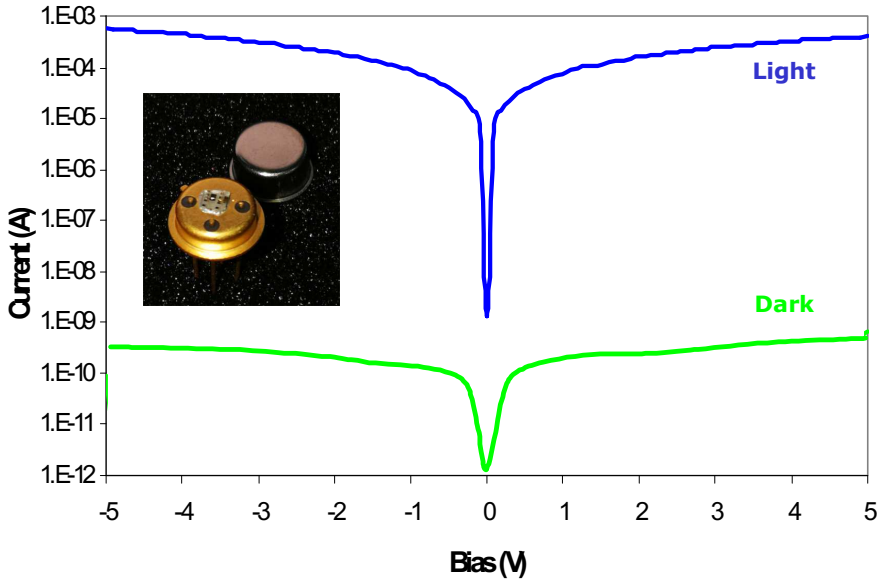

Figure 14 I/V Curves for a packaged SB (Mg)ZnO MSM PD both with and without front illumination (inset shows a photograph of the packaged device). N.B. current is in log scale.

The I/V curves show dark currents of 300 pA (at -5V bias) and over six orders of magnitude of separation between dark and light currents. This is more than was observed before device singulation, mounting and wire connecting (there is both a lower dark current and a higher photocurrent). This may be because of lower contact resistance with bonded contact wires compared to probe arms. The corresponding spectral responsivity curve is shown below.

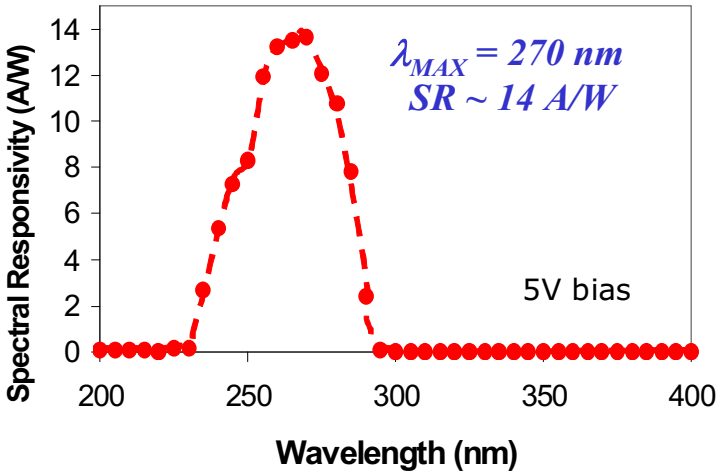

Figure 15 Spectral responsivity for the packaged (Mg)ZnO MSM device shown in Figure 14.

The responsivity curve conforms well to the DVGW standard spectral form (shown in Figure 12). The solar rejection ratio (I_{270} : I_{350}) is over 3 x 10^5 and the peak spectral responsivity (at a bias of 5V) is about 14 A/W (centred at 270 nm). This is more than two decades higher than that for typical commercial SiC based PDs (see Figure 12). Such relatively high gains are commonly observed for oxide MSMs and they are usually attributed to hole trapping at the interface between the layer and the gold electrode [7].

3.2 β-Ga_2O_3

3.2.1 β-Ga_2O_3 Epitaxy

Figure 16 shows a photograph of a typical 2 inch diameter Ga_2O_3/c-Al_2O_3 wafer grown by PLD.

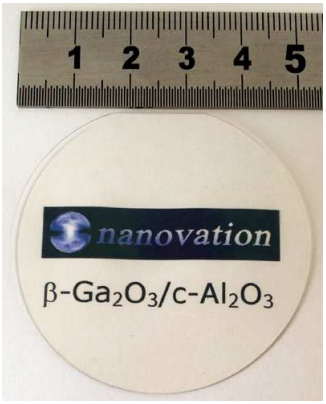

Figure 16 A photograph of a typical (2 inch diameter) Ga_2O_3/c-Al_2O_3 wafer.

The wafer shows good transparency to the visible spectrum and excellent within-wafer homogeneity of the thickness, the SB transmission spectrum and the electrical resistivity. Figure 17 shows the optical transmission spectra for Ga_2O_3 layers of various thicknesses and a plot of the apparent bandgap dependence on film thickness.

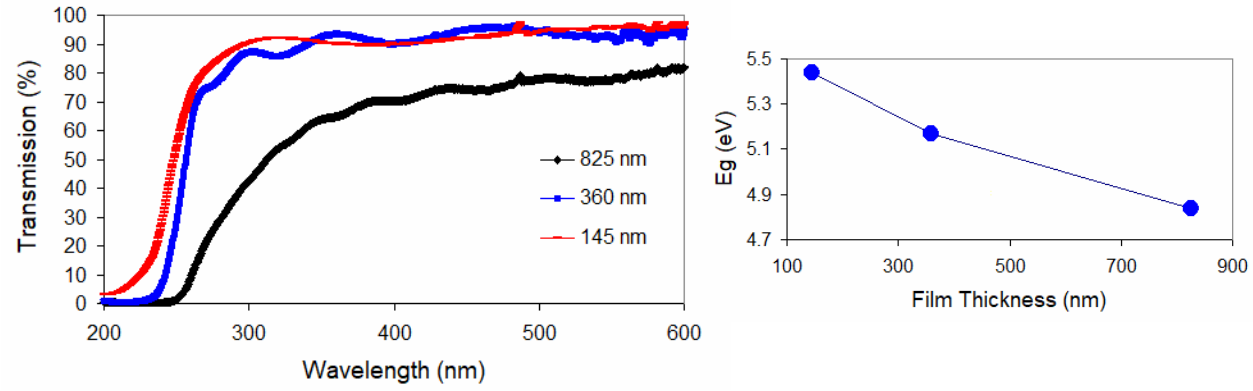

Figure 17 Optical transmission spectra for β-Ga_2O_3 of various thicknesses and a plot of the apparent bandgap dependence on film thickness.

It can clearly be seen that the apparent bandgap decreases with reducing film thickness from a value (typical for β-Ga_2O_3) of ~4.9eV for the 825 nm thick layer to a value of 5.4 eV for a film thickness of 145 nm. This value is much higher than would be expected for β-Ga_2O_3 so XRD study was conducted in order to check that the layer was indeed constituted of β-Ga_2O_3 rather than another Ga_2O_3 polytype [19].

Figure 18 shows a 2θ/Ω XRD scan for the 145 nm thick Ga_2O_3 layer.

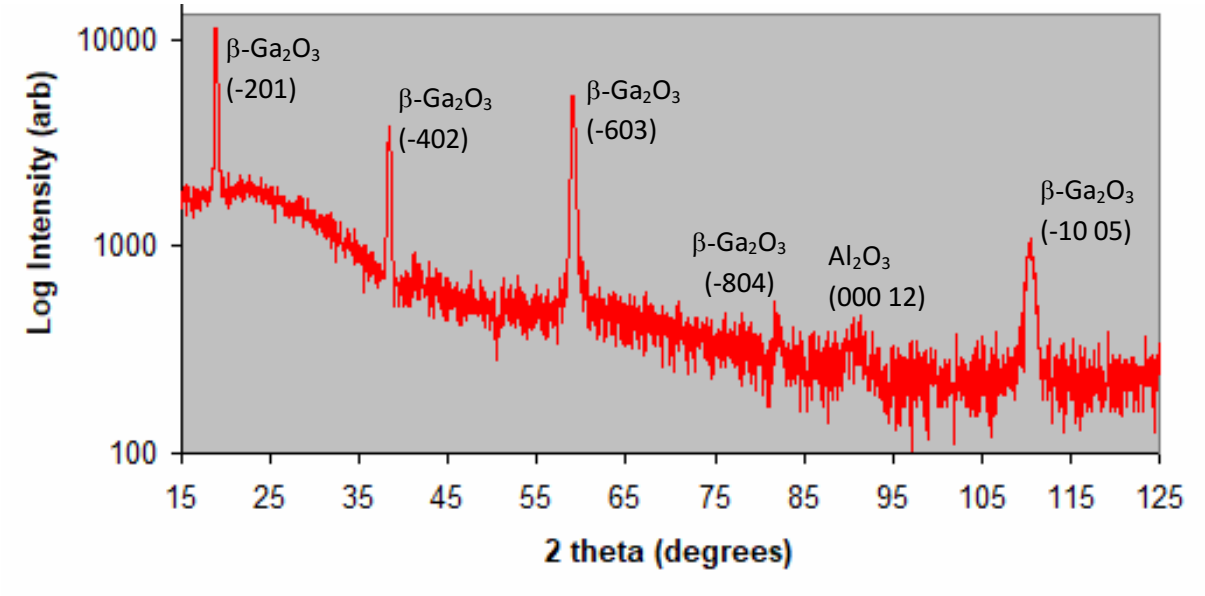

Figure 18 A 2θ/Ω XRD scan for a 145 nm thick Ga_2O_3 layer grown on a c-sapphire substrate.

It can be seen from the scan that the layer shows peaks characteristic of monoclinic β-Ga_2O_3 with a strong preferential (-201) orientation (as is typical for growth on c-sapphire). In particular, there is a clear signature distinguishing the β-Ga_2O_3 polytype from the ε polytype in the (-10 05) peak position i.e. it is centred at about ~110º while the ε polytype would be expected tp exhibit a peak at ~112° and would not have a peak at ~110°. Thus it was concluded that the layer was constituted of β-Ga_2O_3.
Other possible origins of the increase in bandgap with decreasing film thickness are epitaxial strain and/or Al diffusion into the Ga_2O_3 layer from the sapphire substrate [15].

3.2.2 β-Ga_2O_3 Front-End Level 1: MSM Device Processing and Test

Figure 19 shows I/V curves (both with and without back illumination) for an MSM PD made from a 145nm thick β-Ga_2O_3 layer.

The I/V curves show more than four orders of magnitude of separation between dark and light current and a dark current of 250pA (for a bias voltage of -5V).

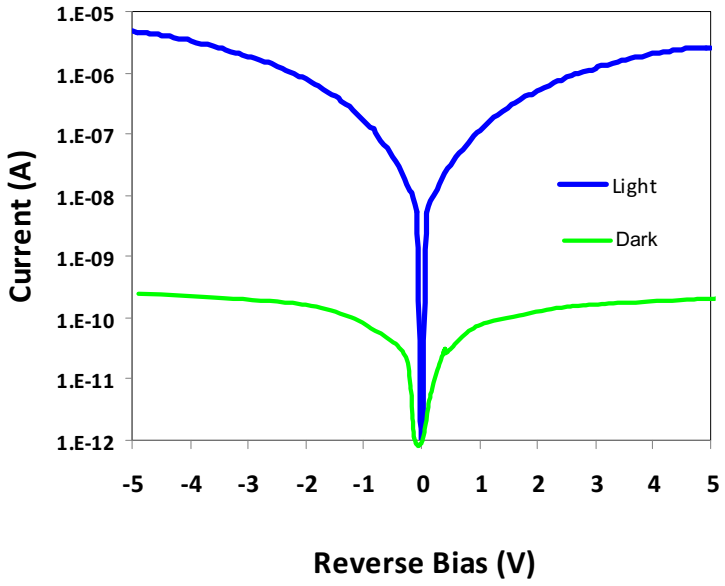

Figure 19 I/V Curves for a β-Ga_2O_3 MSM PD both with and without back illumination (6 micron finger spacing) – N.B. current is in log scale.

Figure 20 shows the spectral responsivities for MSM devices made from the β-Ga_2O_3 layers of three different thicknesses shown in Figure 17.

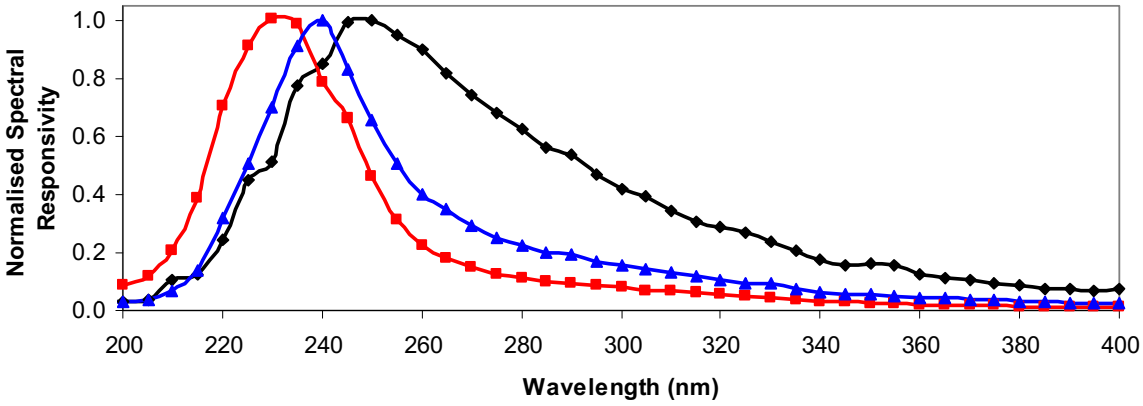

Figure 20 The normalized spectral responsivity as a function of thickness for MSM devices made from the β-Ga_2O_3 layers shown in Figure 17 (bias voltage was -0.75V and finger spacing was 6 microns in all cases).

The peaks of the spectral responsivity are centred at 230, 240 and 250 nm, respectively, for the 145, 360 and 825 nm thick layers. These values correlate closely with the increase in apparent bandgap found in the optical transmission studies (see Figure 17, above).

The absolute peak values of spectral responsivity values (at a bias of -0.75V) were 4.3, 39.5 and 6.0 A/W, respectively.

All three spectra show a significant detection tail extending into the UVB and UVA. This is commonly observed for oxide MSM PDs and is usually attributed to defects in the material [7]. Interestingly the tail is progressively suppressed with increasing film thickness such that the solar rejection ratio (I_{peak} : I_{350}) drops by a factor of 5.9. This drop is similar to the ratio of the respective layer thicknesses, and thus the layer electrical resistances (thinner layers are more electrically resistive). Since the voltage bias across the junctions is fixed, this is consistent with a decreasing current in thinner layers.

Figure 21 shows the time response of the photoresponse at 26.8 Hz for the device shown in Figure 19 (at 5V bias).

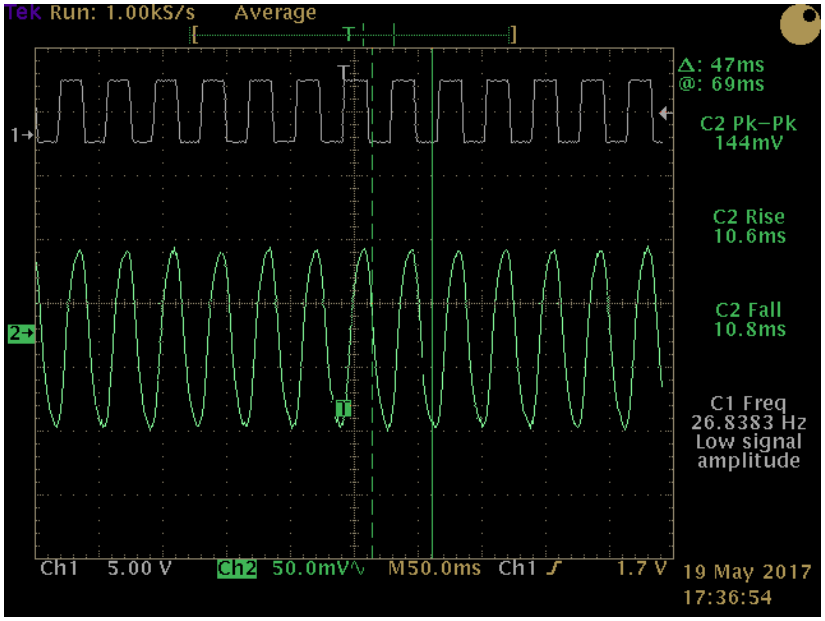

Figure 21 The time dependence of the photoresponse at 26.8 Hz for the β-Ga_2O_3 device shown in Figure 19 (at 5V bias). The upper curve is the input square wave and the bottom curve is the MSM device output.

The device shows rise and fall times of 10.6 and 10.8 ms respectively and thus it is just reaching saturation for 26.8 Hz input pulses (i.e. 37ms pulse width).

In summary, Figure 22 presents the complemetary nature of the optical transmission spectra for single phase hcp MgZnO, β-Ga_2O_3 and fcc MgZnO layers grown by PLD.
The figure shows that, rather conveniently, the β-Ga_2O_3 bandgap range (from ~230 nm to ~ 255 nm) corresponds to the mixed fcc/hcp phase region of (Mg)ZnO (see Figure 4). More globally the figure shows the new oxide paradigm for UV PDs in that the bandgaps of single phase (Mg)ZnO and β-Ga_2O_3 materials can be engineered to cover the whole UVA-UVC spectral range from 200 to 400 nm. This is, in fact, the whole UV detection range of interest since oxygen in the air absorbs light with wavelengths below ~ 200nm.

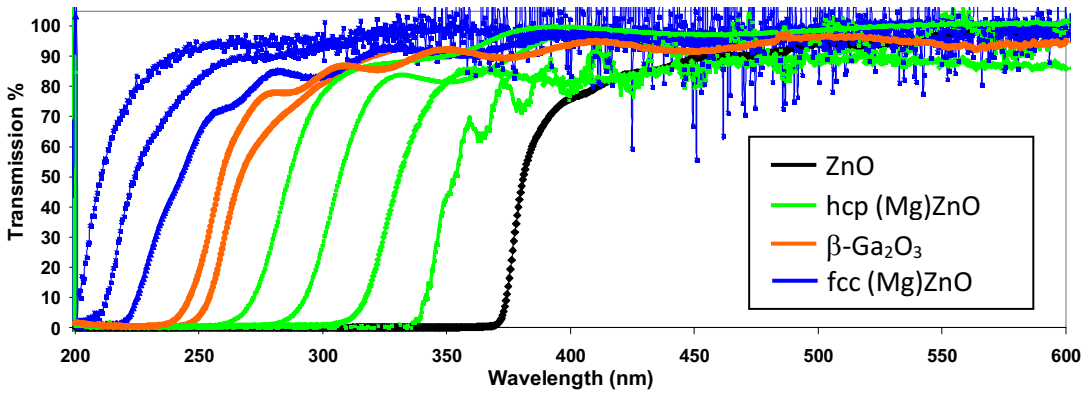

Figure 22 Optical transmission spectra for single phase hcp MgZnO, β-Ga_2O_3 and fcc MgZnO layers grown by PLD.

4. CONCLUSIONS

The bandgap of wurzite ZnO layers grown on 2 inch diameter c-Al_2O_3 substrates by PLD was engineered from 3.7 up to 4.8 eV by alloying with Mg. Above this Mg content the layers transformed from single phase hcp to mixed hcp/fcc phase before becoming single phase fcc above a bandgap of about 5.5 eV.
SB hcp MgZnO MSM PDs with gold IDT were fabricated by single step negative photolithography. They were then singulated and packaged in TO5 cans. The devices gave over 6 orders of magnitude of separation between dark and light signal with solar rejection ratios (I_{270} : I_{350}) of over 3 x 10^5 and dark signals of 300 pA (at a bias of -5V). Spectral responsivities were engineered to fit the "DVGW standard spectral form and gave values of 14 A/W (peaked at 270 nm) for biases of -5 V. This is more than two decades of magnitude higher than the equivalent commercial SiC based device.
Homogeneous Ga_2O_3 layers were also grown on 2 inch diameter c-Al_2O_3 substrates by PLD. Optical transmission spectra were coherent with a bandgap that increased from 4.9 to 5.4 eV when film thickness was decreased from 825 to 145 nm. X-ray diffraction indicated that the films were of the single phase β-Ga_2O_3 monoclinic polytype with strong (-201) orientation. β-Ga_2O_3 MSM detectors gave over 4 orders of magnitude of separation between dark and light signal (at -5V bias) with dark

signals of 250 pA and spectral responsivities of up to 40 A/W (at -0.75V bias). It was found that the spectral responsivity peak position could be decreased from 250 to 230 nm by reducing film thickness from 825 to 145 nm. This shift in peak responsivity wavelength with film thickness (a) was coherent with the apparent bandgap shift that was observed in transmission spectroscopy of the same layers and (b) conveniently provides a coverage of the spectral region in which MgZnO layers show fcc/hcp phase mixing.

ACKNOWLEDGEMENTS

The authors would like to thank Dr. E. Chikoidze of the CNRS Gemac laboratory at the UVSQ (France) for useful discussions, the C2N centre (France) for access to the Panalytical XRD tool and F. Rinaldi of Bruker GmbH (Germany) for help with the XRD measurements of Ga_2O_3.

REFERENCES

[1] R. McClintock, M. Razeghi et al. High quantum efficiency AlGaN solar-blind pin photodiodes Appl. Phys. Lett. 84, 1248 (2004).
[2] M. Razeghi & R. McClintock, "III-Nitride Photodetectors" in Optoelectronic Devices III-Nitride, Razeghi & Henini (2004)
[3] R. McClintock, M. Razeghi et al Solar-Blind Focal Plane Arrays (FPA) based on AlGaN *Appl. Phys. Letts.* 86, 011117 (2005).
[4] E. Cicek, M. Razeghi et al. AlGaN-based deep-UV 320 x 256 FPA *OSA Optics Letts*. 37, 5, 896 (2012)
[5] E. Cicek, M. Razeghi et al. Crack-free AlGaN for SB FPA through reduced area epitaxy *Appl. Phys. Letts. 102, 5 (2013) 051102-1*
[6] Z. Alaie et al Materials Science in Semiconductor Processing 29 (2015) 16
[7] Y. Hou et al. J. Phys. D : Appl. Phys. 47 (2014) 283001
[8] J. L. Yang et al. Chin. Phys. B Vol. 26, No. 4 (2017) 047308
[9] G. C. Hou et al. OPTICS EXPRESS 23 10 (2015) 13556
[10] Z. Ji, J. Du, J. Fan, and W. Wang, "Gallium oxide films for filter and solar-blind UV detector," Opt. Mater. 28(4), 415–417 (2006).
[11] Y. Kokubun, K. Miura, F. Endo, and S. Nakagomi, "Sol-gel prepared β-Ga2O3 thin films for ultraviolet photodetectors," Appl. Phys. Lett. 90(3), 031912 (2007).
[12] T. Oshima, T. Okuno, and S. Fujita, "Ga2O3 thin film growth on c-plane sapphire substrates by molecular beam epitaxy for deep-ultraviolet photodetectors," Jpn. J. Appl. Phys. 46(11), 7217–7220 (2007).
[13 A. Ohtomo *et al.*,] $Mg_xZn_{1-x}O$ as a II–VI widegap semiconductor alloy Appl. Phys. Lett. **72**, 19 (1998) 2466
[14] D. J. Rogers, P. Bove, E. V. Sandana, M. Razeghi and F. Hosseini Teherani ZnO Moves Further into the UV Laser Focus World feature article, 49, 10 October (2013)
[15] $(AlGa)_2O_3$ Solar Blind Photodetectors on Sapphire with Wider Bandgap and Improved Responsivity Q. Feng et al. 2nd International Workshop on Ga_2O_3 and Related Materials, Parma, Italy (2017)
[17] Investigation of MgZnO/ZnO Heterostructures Grown on c-Sapphire Substrates by Pulsed Laser Deposition D. J. Rogers, F. Hosseini Teherani, P. Bove, A. Lusson & M. Razeghi
Proc. of SPIE Vol. 8626 (2013) 86261X-1
[18] A Study into the Impact of Sapphire Substrate Orientation on the Properties of Nominally-Undoped β-Ga2O3 Thin Films Grown by Pulsed Laser DepositionF. H. Teherani, D. J. Rogers, V. E. Sandana, P. Bove, C. Ton-That, L. L. C. Lem, E. Chikoidze, M. Neumann-Spallart, Y. Dumont, T. Huynh, M. R. Phillips, P. Chapon, R. McClintock & M. Razeghi Proc. of SPIE 10105 (2017) 101051R-1
[19] S. I. Stepanov et al. "Gallium Oxide: Properties & Applications" Rev. Adv. Mater. Sci. 44 (2016) 63-86